Thermochimica Acta, 91 (1985) 67–77
Elsevier Science Publishers B.V., Amsterdam – Printed in The Netherlands

KINETICS OF THE THERMAL DECOMPOSITION OF SOME TRANSITION METAL SULFATES

HIROAKI TAGAWA and HIROYUKI SAIJO

Institute of Environmental Science and Technology, Yokohama National University, 156 Tokiwadai, Hodogaya-ku, Yokohama 240 (Japan)

(Received 16 March 1985)

ABSTRACT

The thermal decomposition of sulfates of iron(III), cobalt, nickel, copper and zinc was kinetically studied in flowing nitrogen by use of a thermobalance. Disk-like pellets compacting the anhydrous sulfate powders were used. The decomposition occurred at the phase boundary between the undecomposed sulfate and the oxide product, and the boundary proceeded uniformly from the surface towards the interior. The thickness, x, of the oxide product layer was proportional to the time, t, for $Fe_2(SO_4)_3$, $CoSO_4$ and $NiSO_4$. The x vs. t curves for $CuSO_4$ and $ZnSO_4$ were shown to become two straight lines with a break point. This is due to the formation of their oxysulfate as the intermediate. The ln k vs. $1/T$ relationship moves from lower to higher temperatures in the order: $Fe_2(SO_4)_3$, $CuSO_4$, $CoSO_4$, $NiSO_4$, $ZnSO_4$. The activation energies of the decomposition for sulfates of iron(III), cobalt, nickel, copper and zinc were 212, 217, 257, 211 and 238 kJ mol^{-1}, and those for oxysulfates of copper and zinc at the later stage of the decomposition were 221 and 275 kJ mol^{-1}, respectively. The activation energies were closely related to the enthalpies of decomposition for the sulfates.

INTRODUCTION

The thermal decomposition of metal sulfates has been under recent investigation for a variety of potential applications, for example, possible storage of solar energy or nuclear heat. One of the suggested applications is hydrogen production by thermochemical water-splitting cycles [1], which are performed in a closed system composed of a number of reactions. Many cycles have been proposed so far, and the verification either from the literature or through experimentation has been carried out for the reactions. The cycles, which comprise the catalytic decomposition of sulfuric acid or the thermal decomposition of metal sulfate, where sulfur oxide is used as a recycling agent, are thermodynamically and technologically characterized [2–7]. In particular, the use of metal sulfates is preferable for overcoming the problems allied with the handling and decomposition of sulfuric acid.

The thermal decomposition of metal sulfates has been studied by many

0040-6031/85/$03.30

investigators, but, unfortunately, widely discrepant values are reported for the same compound, and systematic research for their decomposition has not been found. Thus, we studied the thermal decomposition of 16 metal sulfates by thermogravimetry, and found the result that the initial decomposition temperatures of the sulfates were closely related to the decomposition pressures over the sulfates [8]. In the present paper, the kinetics of thermal decomposition for sulfates of iron(III), cobalt, nickel, copper and zinc, which belong to the transition elements, were studied. The kinetic study of the thermal decomposition using the pelletized bulk samples was carried out only by Ingraham and co-workers on $MnSO_4$ [9], $Fe_2(SO_4)_3$ [10], $NiSO_4$ [11] and $CuSO_4$ [12] for the aim of metallurgical applications.

EXPERIMENTAL

Materials

Metal sulfates used were $Fe_2(SO_4)_3 \cdot 13H_2O$, $CoSO_4 \cdot 7H_2O$, $NiSO_4 \cdot 6H_2O$, $CuSO_4 \cdot 5H_2O$ and $ZnSO_4 \cdot 7H_2O$. These sulfates were provided by Kanto Chemical Co. as guaranteed reagent grade. The sulfates were ground in an agate mortar to pass through 200 mesh sieve and heated to change to the anhydrates at 300°C in air, then they were compacted into disk-like pellets, 7 mm in diameter and about 1.5 mm in thickness, at a pressure of 7.8 tonne cm^{-2}. The bulk densities were in the range 60–80% of the theoretical values as described later.

Apparatus and procedures

The apparatus consisted of an electrobalance (Cahn, model 2000) used as a thermobalance, a Kanthal resistance furnace, 35 mm ID and 200 mm in length, a gas supply system and vacuum pumps. A double hook made of platinum wire, 0.5 mm in diameter, was suspended in the heating zone by means of a platinum wire extending from one end of the balance arm. A quartz reaction tube, 20 mm ID and 350 mm in length, was connected to the vacuum bottle containing the balance.

All experiments were carried out using the pelletized samples. After the pellet was loaded onto the hook, high-purity nitrogen ($p_{O_2} < 10^{-6}$ atm) was allowed to flow at 200 cm^3 min^{-1}, heated at 30°C min^{-1} to 300°C and kept at that temperature for 20 min. After dehydration the sample was again heated at 30°C min^{-1} to the desired temperature, and maintained at that temperature until the decomposition finished or for 24 h if it had not finished before that time. For $Fe_2(SO_4)_3$ experiments in flowing air (200 cm^3 min^{-1}) were also performed.

X-ray diffraction (XRD) for all the products and the intermediate com-

pounds was performed by a diffractometer (Rigaku Denki Co., type Rad-1A) with Cu$K\alpha$ radiation monochromatized with a bent graphite crystal.

Calculation of decomposition rate

As known in the thermal decomposition of limestone [13,14] and also found in the decomposition of $Fe_2(SO_4)_3$ by Warner and Ingraham [10], an endothermic reaction of a bulk sample or a compacted pellet proceeds isodimensionally from the surface to the interior. When the cross-section of the pellets, in the present work, was examined at various time intervals during decomposition, it was found that the decomposition occurred along the phase boundary between the undecomposed sulfate and the oxide product, and the interface advanced from the surface towards the interior with nearly the same depth. Thus, the kinetics of the thermal decomposition of the pelletized sample were reduced to determine how the phase boundary moves into the interior.

During the experiments, weight loss due to the decomposition of metal sulfates was measured as a function of time at desired temperatures. The fraction decomposed, α, was calculated from the ratio of the residual weight of SO_3 in the sample after time t, $W(SO_3, t)$, to the initial weight of SO_3 at the beginning of the decomposition, $W(SO_3, t = 0)$, as

$$\alpha = 1 - W(SO_3, t)/W(SO_3, t = 0) \quad (1)$$

The compacted pellet, $2R$ in diameter and $2H$ in thickness, was used, as shown in Fig. 1. The rate of decomposition was calculated from the weight loss of the pellet. The initial weight of SO_3 in the form of sulfate is $8\pi\rho R^2 H$, where ρ is the density of SO_3. When the depth of the interface penetrated from the sample surface is x' at time t after the decomposition occurred, the weight of the remaining SO_3 becomes $8\pi\rho(R - x')^2(H - x')$. Here, it is assumed that the volume is not changed by the decomposition. Equation (1),

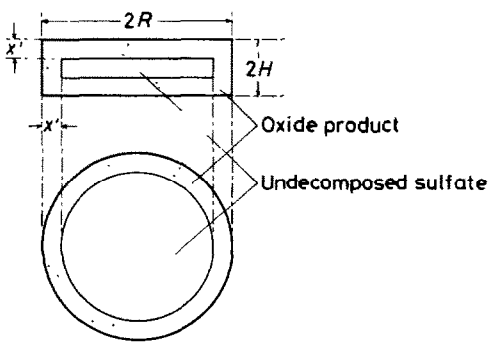

Fig. 1. Schematic diagram of the geometric changes due to the decomposition of a disk-like pellet of the sulfates.

TABLE 1

The ratio of the bulk density to the theoretical, γ, and the cubic root of the ratio, $\gamma_L = \gamma^{1/3}$ for the pellets of metal sulfates

Sulfates	γ	γ_L
$Fe_2(SO_4)_3$	0.73	0.90
$CoSO_4$	0.61	0.85
$NiSO_4$	0.61	0.85
$CuSO_4$	0.68	0.88
$ZnSO_4$	0.76	0.91

therefore, is rewritten as follows

$$1 - \alpha = (1 - x'/R)^2(1 - x'/H) \tag{2}$$

or

$$1 - \alpha = (1/f)^2(f - \xi)^2(1 - \xi) \tag{3}$$

where $f = R/H$ and $\xi = x'/H$. The ξ value, which should be named one-dimensional or linear decomposition ratio, is the fraction decomposed with length. When f and α are given, eqn. (3) can be solved for ξ by numerical calculation by Newton's method. In order to compare the decomposition rate of metal sulfates with different bulk density, the apparent bulk density should be corrected to the theoretical density because the pellet was made by compacting fine powders of anhydrous sulfate. The ratio of filling, γ, which is defined as the ratio of the bulk density to the theoretical density, was introduced. As the decomposition rate was expressed as a function of the depth of the interface penetrated, the cubic root of the ratio of filling, $\gamma_L = \gamma^{1/3}$, was used instead of γ. When the ξ value is used to express the degree of the decomposition, the true thickness of the product layer becomes

$$x = \gamma_L x' \text{ or } x = \gamma_L \xi H \tag{4}$$

The γ and γ_L values for the sulfates used are shown in Table 1.

RESULTS AND DISCUSSION

Decomposition rates of the sulfates

Figure 2 shows the relationship between fraction decomposed and time at various temperatures for iron(III) sulfate. For other sulfates, similar curves were obtained. In these experiments, a nitrogen flow rate of 200 $cm^3\ min^{-1}$ was used. The linear flow rate on the sample surface was 64 $cm\ min^{-1}$ at room temperature. The decomposition rates were not affected in a nitrogen flow above 150 $cm^3\ min^{-1}$. Another factor affecting the decomposition rates is the pressure compacting the sample powders. The decomposition rates

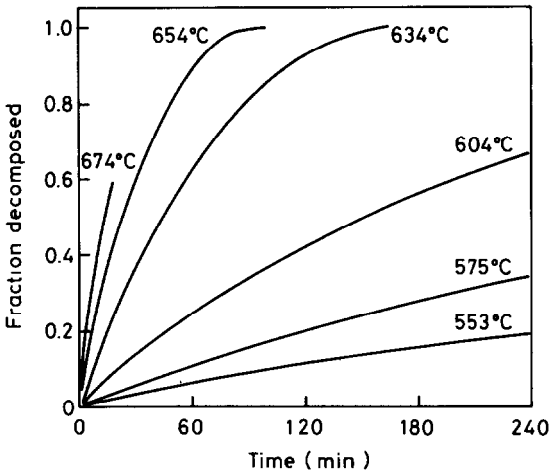

Fig. 2. Relationship between fraction decomposed and time for $Fe_2(SO_4)_3$ in high-purity nitrogen flowing at 200 cm^3 min^{-1}.

were examined as a function of pressure, and it was confirmed that the rate was not affected above 5.2 tonne cm^{-2}. A pressure of 7.8 tonne cm^{-2} was used.

To determine the mechanism of the thermal decomposition, the way the thickness of the product layer, calculated by use of eqn. (3), varied with time was analyzed. The following three models were considered: the rate of decomposition is controlled either by (1) the decomposition at the reaction interface; (2) the diffusional transport of gaseous products through solid product layer; or (3) the combination of mechanisms (1) and (2), where both rates are comparable. Mechanism (1), where the decomposition rate is proportional to the area of the interface, was observed in the decomposition of manganese [9], iron(III) [10], nickel [11] and copper sulfates [12], and limestone [13,14]. Mechanism (3) was found in the decomposition of limestone composed of fine grains [15]. The reaction mechanisms can be simply given by the following expressions:

(1) decomposition controlled by chemical reaction at the phase boundary

$$dx/dt = k_C \text{ or } x = k_C t \tag{5}$$

(2) decomposition controlled by diffusion

$$dx/dt = x/k_D \text{ or } x^2 = (k_D/2)t \tag{6}$$

(3) combination of mechanisms (1) and (2)

$$2x^2/k_D + x/k_C = t \tag{7}$$

The mechanism can be determined by plotting x against t or t/x.

Figure 3 shows the relationship between depth of the product layer

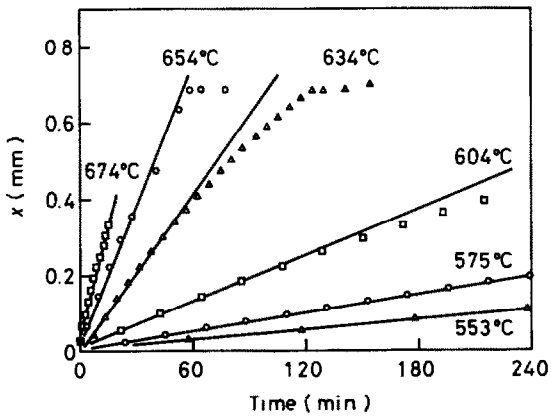

Fig. 3. Relationship between thickness of the product layer and time for $Fe_2(SO_4)_3$ in high-purity nitrogen flowing at 200 cm^3 min^{-1}.

formed toward the interior and time for $Fe_2(SO_4)_3$. The x values were calculated from the data shown in Fig. 2 and Table 1. The curves were nearly linear at any temperature. This means that the overall decomposition rate is chemically determined by mechanism (1). The slopes of the lines in Fig. 3 give the reaction rate, k_C. The x vs. t curves for $Fe_2(SO_4)_3$ in flowing air and those for $CoSO_4$ and $NiSO_4$ were linear. The curves for $CuSO_4$ and $ZnSO_4$, however, did not consist of one straight line, but were approximately shown by two straight lines with a break point. The x vs. t curves of the decomposition of $CuSO_4$ are shown in Fig. 4. Two decomposition rates were obtained from the curves at any temperature. This, as mentioned below, is thought to come from the formation and decomposition of the oxysulfate as the intermediate compound.

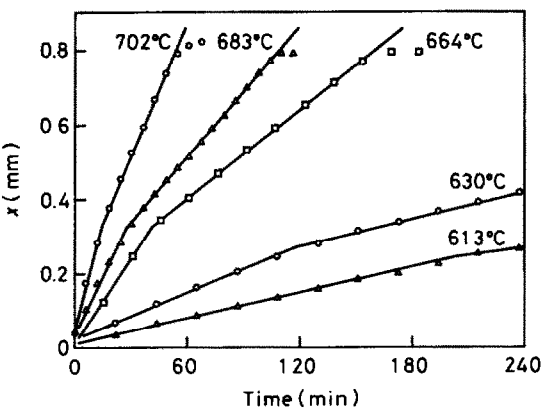

Fig. 4. Relationship between thickness of the product layer and time for $CuSO_4$ in high-purity nitrogen flowing at 200 cm^3 min^{-1}.

Constitution of the product layer during decomposition

In order to clarify the reason why the x vs. t curves consist of two straight lines with a break point for the sulfates of copper and zinc, the phases formed during and after the decomposition were examined by XRD for all the sulfates. Sulfates of iron(III) and nickel have no intermediate compound. Their products were surely only the oxides. Therefore, the phase composition during the decomposition was the undecomposed sulfate and the oxide product.

In the cobalt–oxygen system there are two oxides: CoO and Co_3O_4. Which oxide is produced by the decomposition of cobalt sulfate depends on the oxygen partial pressure over the sample. From calculation using the thermodynamic tables [16,17], it is known that Co_3O_4 is more stable than CoO in the presence of the gaseous product, SO_3, SO_2 and O_2 at temperatures below 1100°C, but CoO becomes more stable than Co_3O_4 in flowing high-purity nitrogen above 550°C. Figure 5 shows XRD patterns of the sample taken during the course of the decomposition. From the results and thermodynamic considerations, it is deduced that the decomposition occurred to form Co_3O_4, then the Co_3O_4 was further changed into CoO from

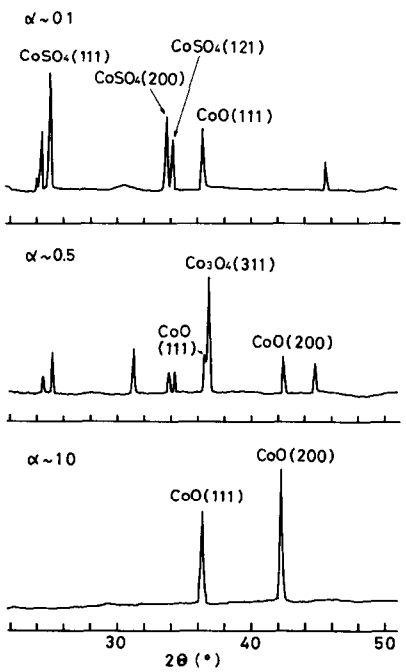

Fig. 5. XRD patterns of the products for the decomposition of $CoSO_4$ at ~0.1, ~0.5 and ~1.0 of the fraction decomposed.

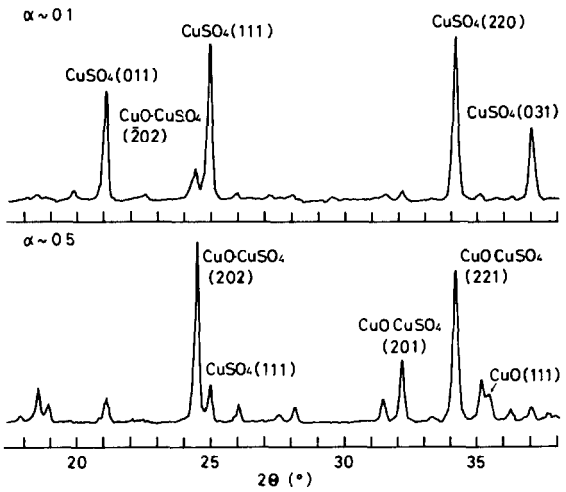

Fig. 6. XRD patterns of the products for the decomposition of $CuSO_4$ at ~ 0.1 and ~ 0.5 of the fraction decomposed.

the pellet surface. The product layer during the decomposition was constituted by $CoSO_4/Co_3O_4/CoO$.

The decomposition of sulfates of copper and zinc yielded their oxysulfates. For copper sulfate the colored oxysulfate intermediate was observed even with the eyes. The cross-section of the pellets during decomposition consisted of three different colored layers, as $CuSO_4/CuO \cdot CuSO_4/CuO$. Figure 6 shows XRD patterns of the samples taken during the course of decomposition. For zinc sulfate, the XRD patterns of the samples also showed the intermediate compound to exist, as in the case of copper sulfate. The decomposition pressure of the metal sulfate is generally higher than that of the oxysulfate at any temperature. Consequently, the decomposition proceeds successively if the decomposition rates of the sulfate and oxysulfate correspond to their pressures, respectively: the first step is the decomposition of the sulfate to the oxysulfate, and the second is that of the oxysulfate to the oxide. As shown in Fig. 4, the x vs. t curves for $CuSO_4$ consisted of two straight lines with a break point. The product was only the oxysulfate at the early stage, and the curve was made by the decomposition of the sulfate to the oxysulfate. When the oxysulfate layer is thickened with time, the decomposition of the oxysulfate occurs from the surface, and the overall decomposition is governed by the decomposition rate of the oxysulfate.

Activation energy of the decomposition

Figure 7 shows the relationship between the logarithm of the decomposition rate and the reciprocal of the absolute temperature for the sulfates used. The decomposition of sulfates of copper and zinc yielded two straight lines

with a break. The ln k vs. $1/T$ plots are seen to move from lower to higher temperatures in the following order: $Fe_2(SO_4)_3$, $CuSO_4$, $CoSO_4$, $NiSO_4$, $ZnSO_4$.

The activation energy is calculated according to the Arrhenius equation

$$k = C \exp(-Q/RT) \tag{8}$$

where k is the reaction rate, C a constant, Q the activation energy and R the gas constant. The slope of each line shown in Fig. 7 gives the activation energy for the decomposition. The activation energies of decomposition for sulfates of iron(III), cobalt, nickel, copper and zinc were 211.8 ± 0.8, 216.5 ± 1.5, 256.6 ± 6.8, 210.6 ± 3.0 and 238.1 ± 2.3 kJ mol^{-1}, respectively, and those for sulfates, probably oxysulfates, of copper and zinc at the later stage on the x vs. t curves were 221.0 ± 2.3 and 274.8 ± 2.1 kJ mol^{-1}, respectively.

When an endothermic reaction such as the decomposition of sulfates or carbonates occurs, the energy required is supplied from the surroundings to the reaction interface through the product layer. Although mechanism (1) can be applied to the endothermic reactions in many cases, actually the flow of heat is important for the reaction to proceed. The activation energy of the endothermic reaction could be related to the enthalpy change of the reaction. Figure 8 shows the relationship between the activation energies of the decomposition of the sulfates and the standard enthalpy changes at 298.15 K, ΔH^0_{d298}, where the enthalpies were taken from the table in a previous

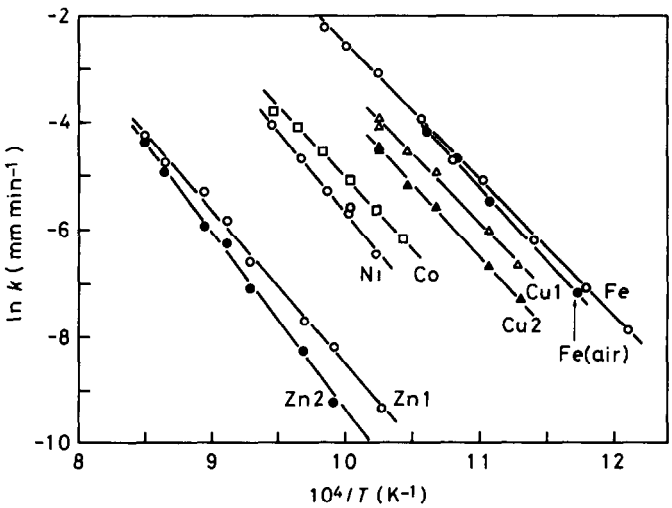

Fig. 7. Relationship between the logarithm of the decomposition rate and the reciprocal absolute temperature for sulfates of iron(III), cobalt, nickel, copper and zinc in high-purity nitrogen flowing at 200 cm^3 min^{-1}. Fe(air) shows the decomposition in air flowing at 200 cm^3 min^{-1}. Numbers 1 and 2 for Cu and Zn show the earlier and later stages of the x vs. t curves for $CuSO_4$ and $ZnSO_4$, respectively.

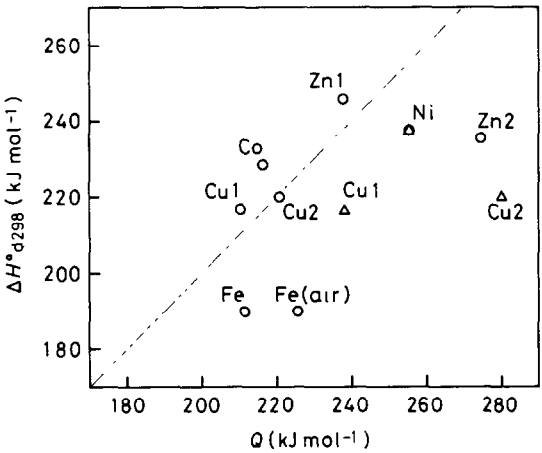

Fig. 8. Relationship between the standard enthalpy of decomposition at 298.15 K, ΔH_{d298}, and the activation energy, Q, for sulfates of iron(III), cobalt, nickel, copper and zinc in high-purity nitrogen flowing at 200 cm^3 min^{-1}. Fe(air) shows the decomposition in air flowing at 200 cm^3 min^{-1}. △ shows the results obtained by Ingraham and Marier [11,12].

report [8]. The activation energies observed by Ingraham and Marier [11,12] are also shown in the figure. Their value for $Fe_2(SO_4)_3$ was 83 kJ mol^{-1} [10], which was out of the scale in the figure. The activation energies are seen to be close to the enthalpies of the decomposition. If the experimental activation energy for the endothermic reaction is divided into the energy thermodynamically required for the reaction to occur and that kinetically required for activating the reaction complex, in the present case, it will be shown that the latter energy is close to zero.

REFERENCES

1 J.E. Funk and R.M. Reinstrom, Ind. Eng. Chem. Process Des. Dev., 5 (1966) 336.
2 L.A. Booth and J.D. Balcom, LA-5456-MS (1973).
3 G.E. Besenbruch, K.H. McCorkle, J.H. Norman, D.R. O'Keefe, J.R. Schster and M. Yoshimoto, Proc. 3rd World Hydrogen Energy Conf., Tokyo, Pergamon Press, Oxford, 1980, p. 243.
4 P.W.T. Lu and R.L. Ammon, Proc. 3rd World Hydrogen Energy Conf., Tokyo, Pergamon Press, Oxford, 1980, p. 439.
5 S. Mizuta and T. Kumagai, Bull. Chem. Soc. Jpn., 55 (1982) 1939.
6 S. Shimizu, S. Sato, Y. Ikezoe and H. Nakajima, Denki Kagaku (J. Electrochem. Soc. Jpn.), 49 (1981) 699.
7 K.E. Cox, W.M. Jones and C.L. Peterson, 3rd World Hydrogen Energy Conf., Tokyo, Pergamon Press, Oxford, 1980, p. 345.
8 H. Tagawa, Thermochim. Acta, 80 (1984) 23.
9 T.R. Ingraham and P. Marier, Trans. Metall. Soc. AIME, 242 (1968) 2039.
10 N.A. Warner and T.R. Ingraham, Can. J. Chem. Eng., 40 (1962) 263.
11 T.R. Ingraham, Trans. Metall. Soc. AIME, 236 (1966) 1067.

12 T.R. Ingraham and P. Marier, Trans. Metall. Soc. AIME, 233 (1965) 363.
13 C.C. Furnas, Ind. Eng. Chem., 23 (1931) 534.
14 H. Tagawa and B. Sudo, Kogyo Kagaku Zasshi (J. Chem. Soc. Jpn. Ind. Eng. Sect.), 61 (1958) 946.
15 H. Tagawa, Kogyo Kagaku Zasshi, (J. Chem. Soc. Jpn. Ind. Eng. Sect.), 64 (1961) 1759.
16 D.D. Wagman, W.H. Evans, V.B. Parker, R.H. Schumm, I. Halow, S.M. Bailey, K.L. Churney and R.L. Nuttall, The NBS Table of Chemical Thermodynamic Properties; Selected Values for Inorganic and C1 and C2 Organic Substances in SI Units, J. Phys. Chem. Ref. Data, 11 (Suppl. No 2) (1982).
17 I. Barin and O. Knacke, Thermochemical Properties of Inorganic Substances, Verlag Chemie, Weinheim, 1973; I. Barin, O. Knack and O. Kubaschewski, Suppl., 1977.